VALERI PROJECT

Website: http://www.avignon.inra.fr/valeri

CAMPAIGN 2002

GROUND DATA PROCESSING & PRODUCTION OF THE LEVEL 1 HIGH RESOLUTION MAPS

VALERI 2002

TURCO site
(shrubs)

Philippe Rossello, Marie Weiss

January 2006

CONTENTS

1. Introduction

This report describes the production of the high resolution, level 1, biophysical variable maps for the Turco site in 2002 (see campaign report for more details about the site and the ground measurement campaign: annex or http://www.avignon.inra.fr/valeri). Level 1 map corresponds to the map derived from the determination of a transfer function between reflectance values of the SPOT image acquired during (or around) the ground campaign, and biophysical variable measurements (hemispherical images). For each Elementary Sampling Unit (ESU), the hemispherical images were processed using the CAN-EYE software (Version 4.1) developed at INRA-CSE. The derived biophysical variable maps are:

• four Leaf Area Index (LAI) are considered: effective LAI (LAIeff) and true LAI (LAItrue) derived from the description of the gap fraction as a function of the view zenith angle; effective LAI57 (LAI57eff) and true LAI57 (LAI57true) derived from the gap fraction at 57.5°, which is independent on the leaf inclination. Effective LAI and effective LAI57 do not take into account clumping effect. LAItrue and LAI57true are derived using the method proposed by Lang and Yueqin[1] (1986);

• cover fraction (fCover): it is the percentage of soil covered by vegetation. To improve the spatial sampling, fCover was computed over 0 to 10° zenith angle;

• fAPAR: it is the fraction of Absorbed Photosynthetically Active Radiation (PAR=400-700nm). The fAPAR is defined either instantaneously (for a given solar position) or integrated all over the day. Following a study based on radiative transfer model simulations, it has been shown that the root mean square error between instantaneous fAPAR computed every 30 minutes and the daily fAPAR is the lowest for instantaneous fAPAR at 10h00 AM (solar time, RMSE = 0.021). Therefore, the derivation of fAPAR from CAN-EYE corresponds to the instantaneous black sky fAPAR at 10h00 AM.

The land cover is mainly composed of shrubs. This flat site is at about 3800 m altitude (for more information, see annex or campaign report: http://www.avignon.inra.fr/valeri).

The site coordinates are described in Table 1:

	UTM 19, South, PSAM56 (units = meters)		Geographic Lat/Lon WGS84 (units = degrees)	
	Northing	Easting	Lat.	Lon.
Upper left corner	7985000	584000	-68.20748367	-18.22591569
Lower right corner	7982000	587000	-68.17898478	-18.25290831
Center	7983500	585500	-68.19323532	-18.23941258

Table 1. Description of the site coordinates.

2. Available data

2.1. SPOT Image

The SPOT image was acquired the 29th August 2002 by HRVIR1 on SPOT4 while the ground measurements were carried out from 25/08/2002 to 30/08/2002. It was geo-located by SPOTimage (level 1B). The projection is UTM 19 South, PSAM56 (please, refer to the campaign report for more details: annex or http://www.avignon.inra.fr/valeri). No atmospheric correction was applied to the image since no atmospheric data were available. However, as the SPOT image is used to compute empirical relationships between reflectance and biophysical variable, we can assume that the effect of the atmosphere is the same over the whole 3 x 3 km site. Therefore, it will be taken into account everywhere in the same way.

Figure 1 shows the relationship between Red and near infrared (NIR) SPOT channels: the soil line is well marked and no saturated points are observed.

---

[1] Lang, A.R.G. and Yueqin, X., 1986. Estimation of leaf area index from transmission of direct sunlight in discontinuous canopies. Agric. For. Meteorol., 37: 229-243.
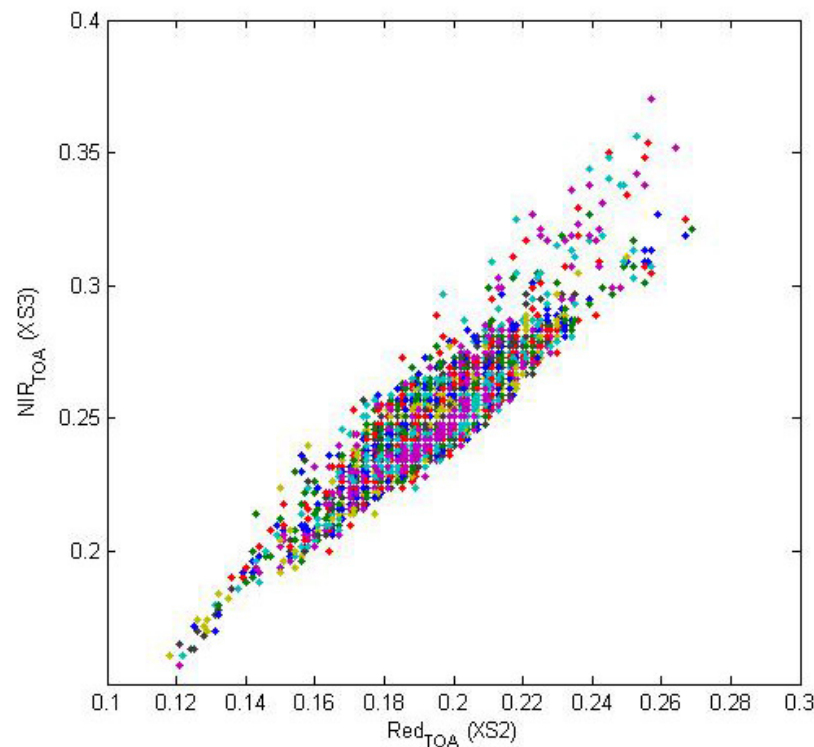
Figure 1. Red/NIR relationship on the SPOT image for Turco, 2002.

2.2. Hemispherical images

The hemispherical images were processed using the CAN-EYE software (Version 4.1) to derive the biophysical variables. Figure 2 and Figure 3 show the distribution of the several variables over the 32 sampled ESUs. As Turco is a 'shrubs' site, all the hemispherical images were acquired from above the canopy. The biophysical variable values are very low with effective LAI lower than 0.13 ant true LAI lower 0.22. Note that the CAN-EYE software (V4.1) provides LAIeff values with a resolution of 0.1: two LAIeff values are available (Figure 2). Therefore, LAItrue, LAI57eff and LAI57true for which the resolution is 0.01 will be used.

True LAI derived from directional gap fraction and true LAI derived from gap fraction at 57.5° are consistent (Figure 2 and Figure 3). Note that LAI57eff varies from 0.01 to 0.12, while LAI57true varies from 0.02 to 0.21. This is due to the clumping observed for several ESUs. This range shows a very homogeneous site in terms of LAI. The relationship between fAPAR and LAI is in agreement with what is expected (Beer-Lambert law) while the fCover-LAI relationship is more noisy.
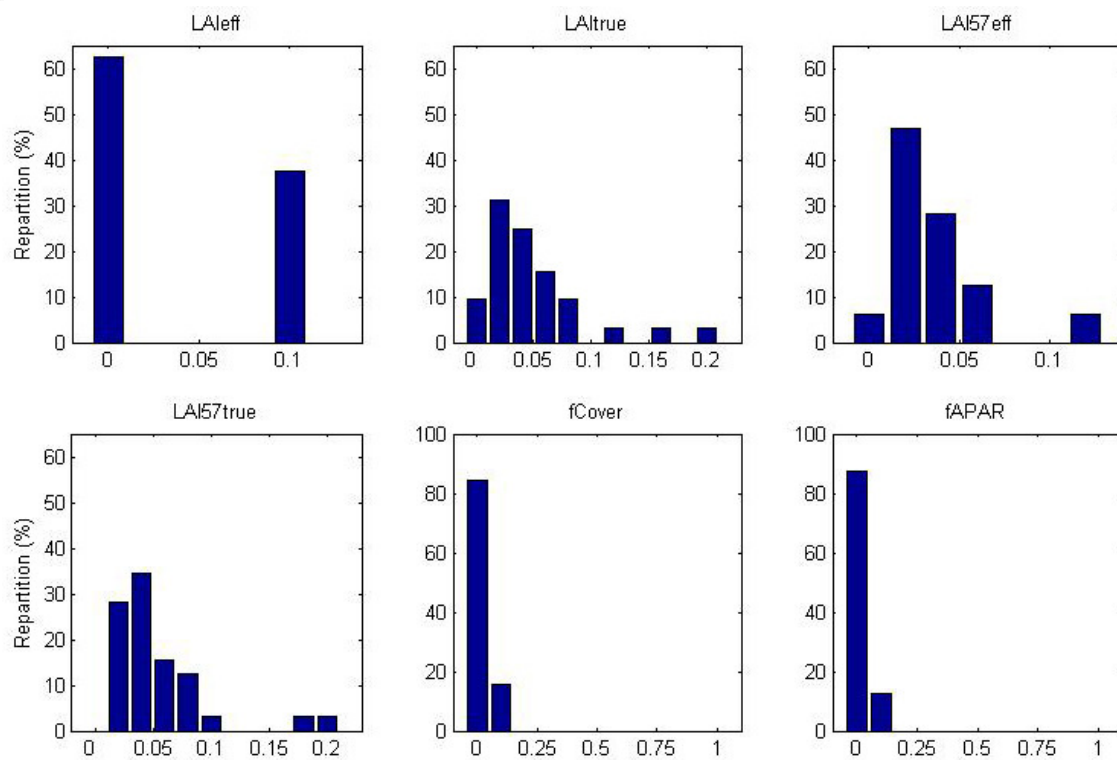
Figure 2. Distribution of the measured biophysical variables over the ESUs.
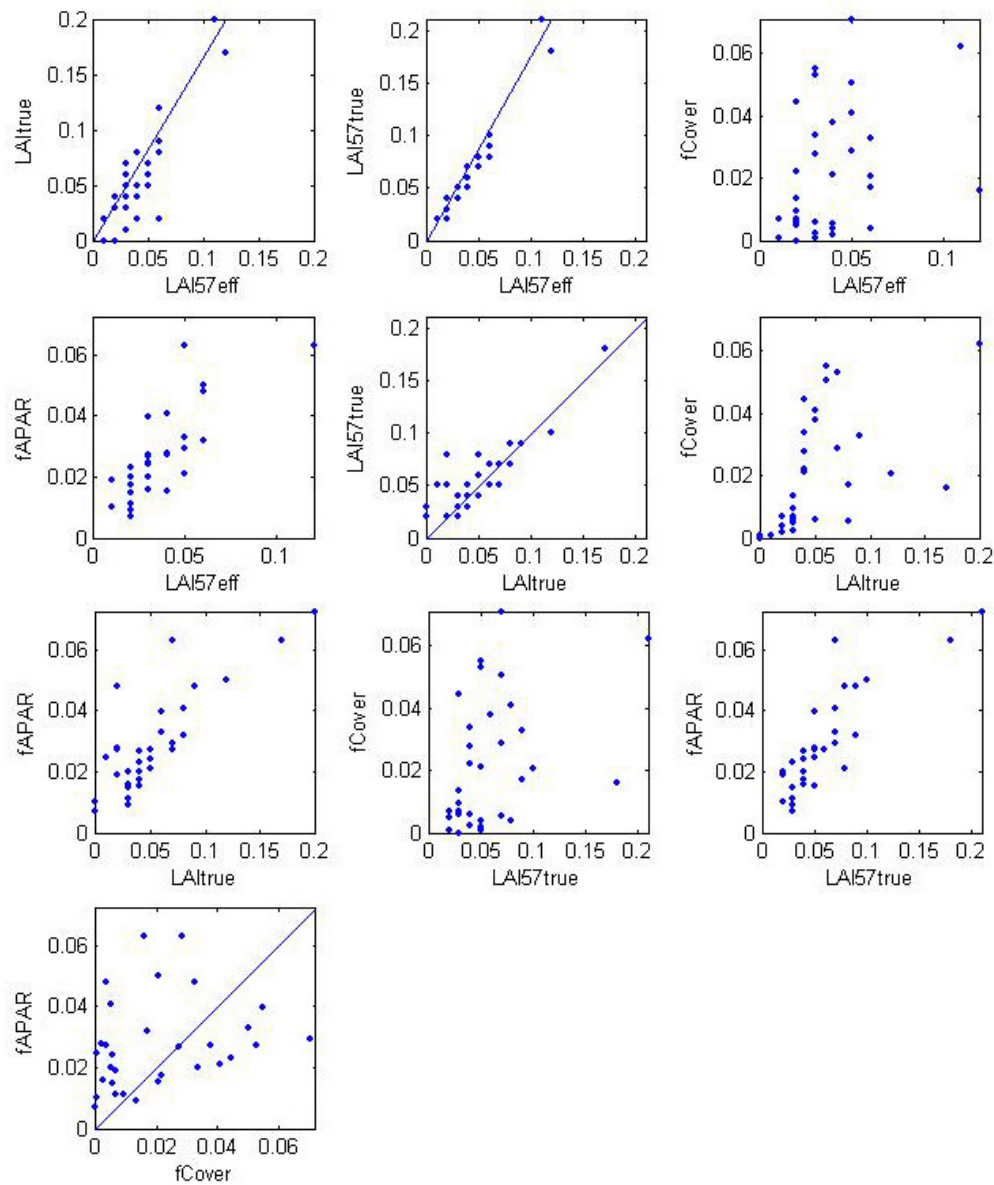
Figure 3. Relationships between the different biophysical variables

2.3. Sampling strategy

2.3.1. Principles

The sampling strategy is defined in the campaign report: annex or http://www.avignon.inra.fr/valeri. The sampling of each ESU is based on twelve elementary photographs.

Figure 4 shows that the 32 ESUs are evenly distributed over the site (3 x 3 km). All the ESUs have been kept for the computation of the transfer function.
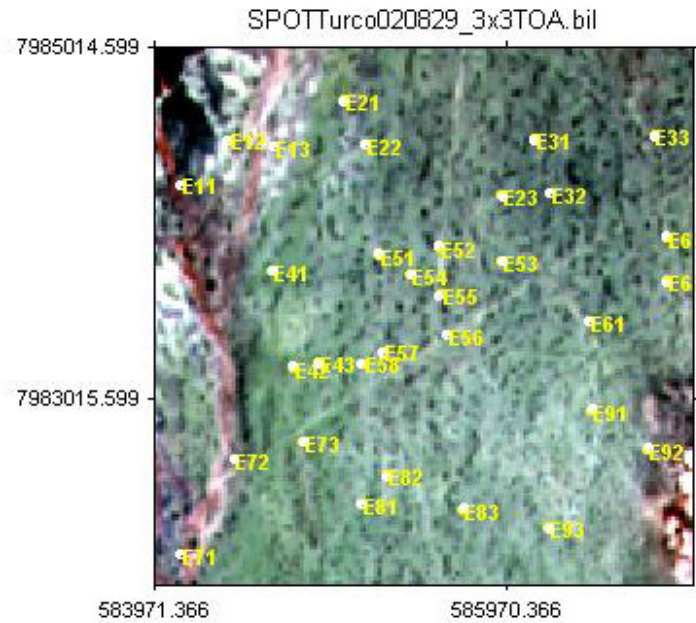
Figure 4. Distribution of the ESUs around the Turco site.

2.3.2. Evaluation based on NDVI values

The sampling strategy is evaluated using the SPOT image by comparing the NDVI distribution over the site with the NDVI distribution over the ESUs (Figure 5). As the number of pixels is drastically different for the ESU and whole site (WS=22500 in case of a 3 x 3 km SPOT image), it is not statistically consistent to directly compare the two NDVI histograms. Therefore, the proposed technique consists in comparing the NDVI cumulative frequency of the two distributions by a Monte-Carlo procedure which aims at comparing the actual frequency to randomly shifted sampling patterns. It consists in:

1. computing the cumulative frequency of the N pixel NDVI that correspond to the exact ESU locations;
2. then, applying a unique random translation to the sampling design (modulo the size of the image);
3. computing the cumulative frequency of NDVI on the randomly shifted sampling design;
4. repeating steps 2 and 3, 199 times with 199 different random translation vectors.

This provides a total population of $N = 199 + 1$(actual) cumulative frequency on which a statistical test at acceptance probability $1 - \alpha = 95\%$ is applied: for a given NDVI level, if the actual ESU density function is between two limits defined by the $N\alpha / 2 = 5$ highest and lowest values of the 200 cumulative frequencies, the hypothesis assuming that WS and ESU NDVI distributions are equivalent is accepted, otherwise it is rejected.
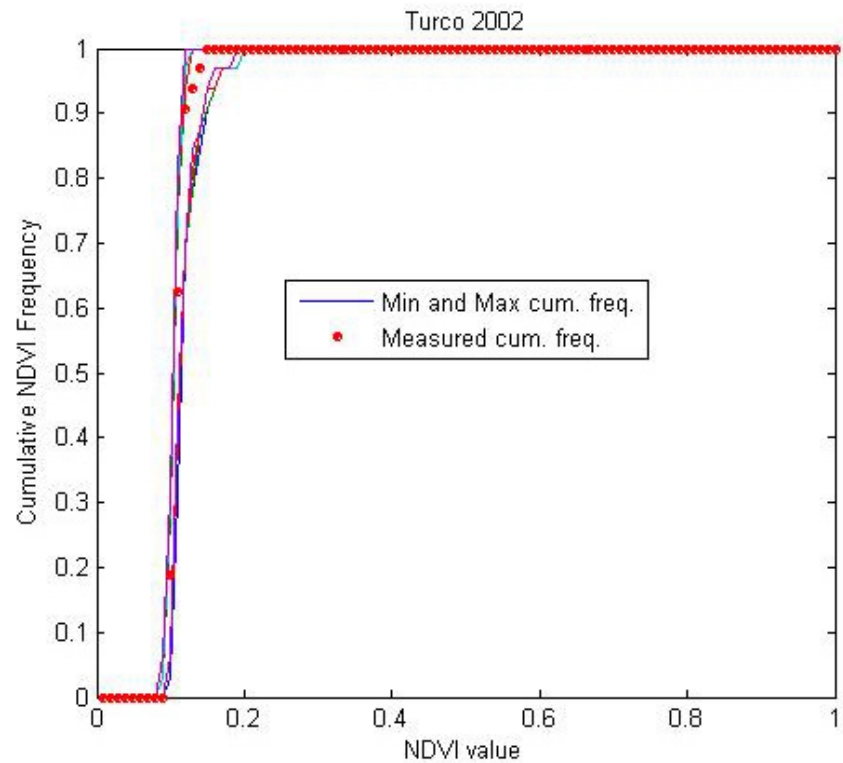
Figure 5. Comparison of the ESU NDVI distribution and the NDVI distribution over the whole image.

Figure 5 shows that the NDVI distribution of the 32 ESUs is good over the whole site (comprised between the 5 highest and lowest cumulative frequencies). Note that NDVIs lower than 0.09 have not been sampled either although they are present in the image. They correspond to bare soil. The site is very homogeneous in terms of NDVI since the highest and lowest distributions are very close.

2.3.3. Evaluation based on classification

A non supervised classification based on the k_means method (Matlab statistics toolbox) was applied to the reflectance of the SPOT image to distinguish if different behaviours on the image for the biophysical variable-reflectance relationship exist.

A number of 4 classes was chosen (Figure 6). The distribution of the classes on the image and on the ESUs is quite comparable. Class 3 is under-represented while classes 1 and 4 appear to be over-sampled. The class 2 is equivalent.
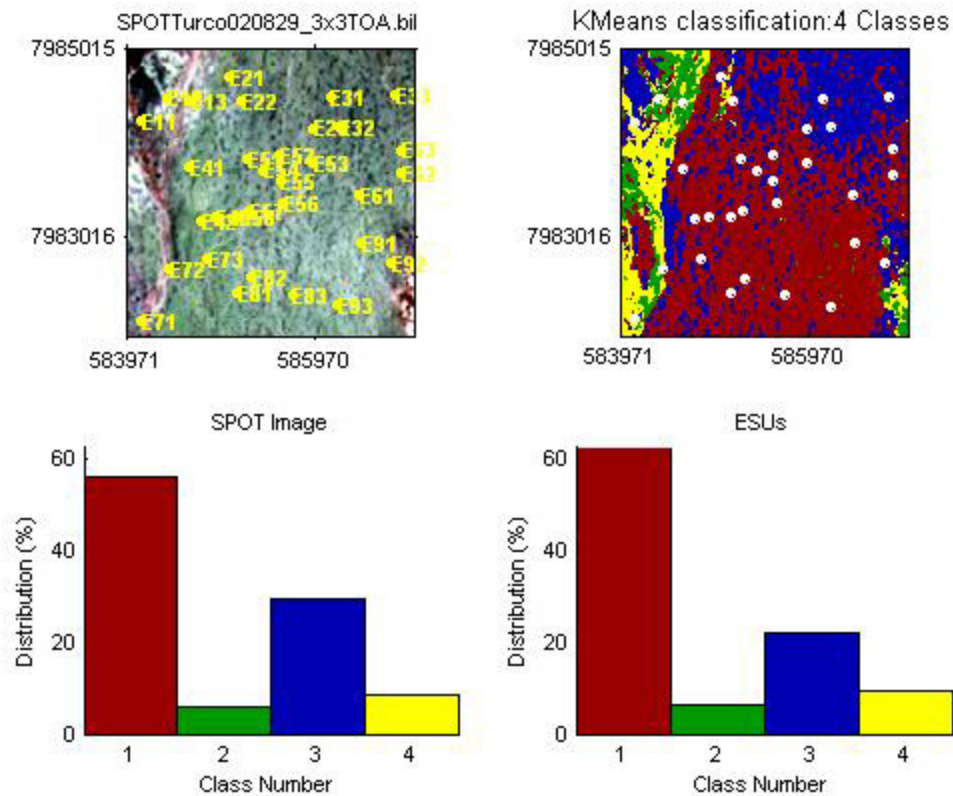
Figure 6. Classification of the SPOT image. Comparison of the class distribution between the SPOT image and sampled ESUs.

Figure 7 shows the different relationships observed between the biophysical variables and the corresponding NDVI on the ESUs, as a function of the SPOT classes determined from non supervised classification.
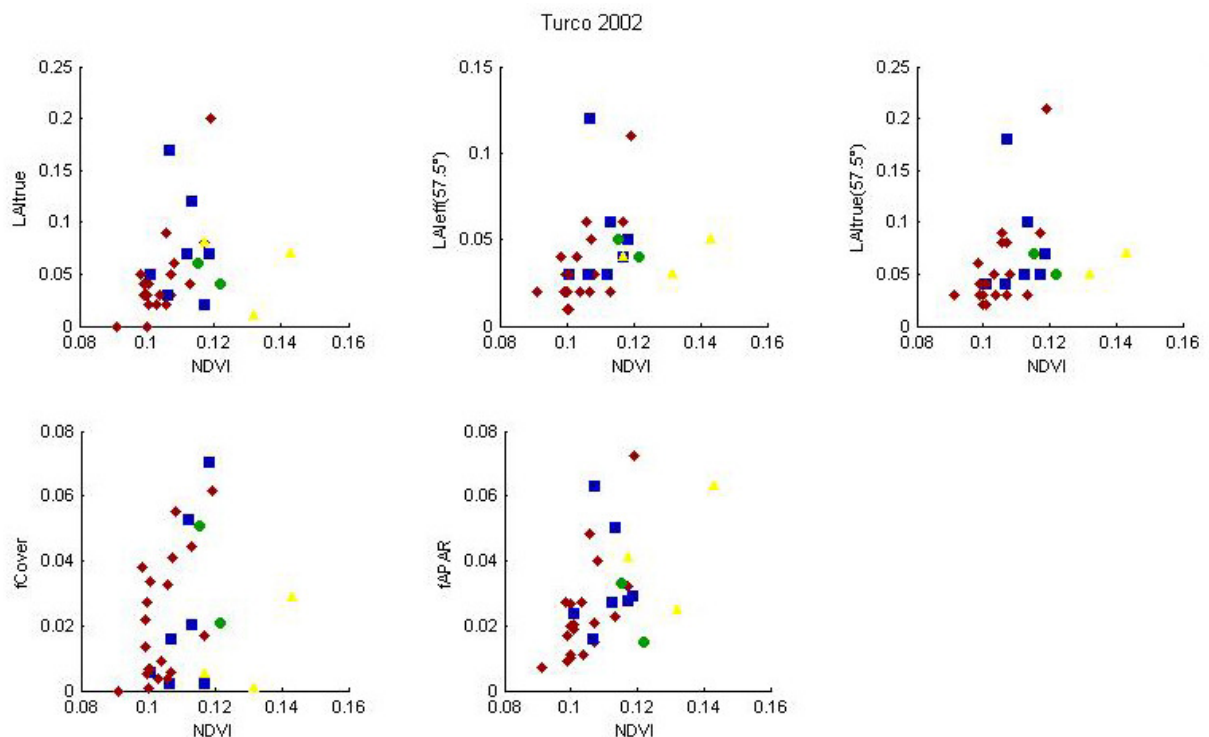

Figure 7. NDVI-Biophysical Variable relationships as a function of SPOT classes

No different behaviour between the classes can be observed, even if two ESUs (E33 in blue class and E92 in red class) differ from the others: LAI values are relatively high compared with NDVI values. Therefore, a single transfer function per variable will be generated.

2.3.4.   Using convex hulls

A test based on the convex hulls was also carried out to characterize the representativeness of ESUs. Whereas the evaluation based on NDVI values uses two bands (red and NIR), this test uses the four bands of the SPOT image. A flag image, is computing over the reflectances (Figure 8). The result on convex-hulls can be interpreted as:

● pixels inside the 'strict convex-hull': a convex-hull is computed using all the SPOT reflectance corresponding to the ESUs belonging to the class. These pixels are well represented by the ground sampling and therefore, when applying a transfer function the degree of confidence in the results will be quite high, since the transfer function will be used as an interpolator;

● pixels inside the 'large convex-hull': a convex-hull is computed using all the reflectance combination (±5% in relative value) corresponding to the ESUs. For these pixels, the degree of confidence in the obtained results will be quite good, since the transfer function is used as an extrapolator (but not far from interpolator);

● pixels outside the two convex-hulls: this means that for these pixels, the transfer function will behave as an extrapolator which makes the results less reliable. However, having a priori information on the site may help to evaluate the extrapolation capacities of the transfer function.
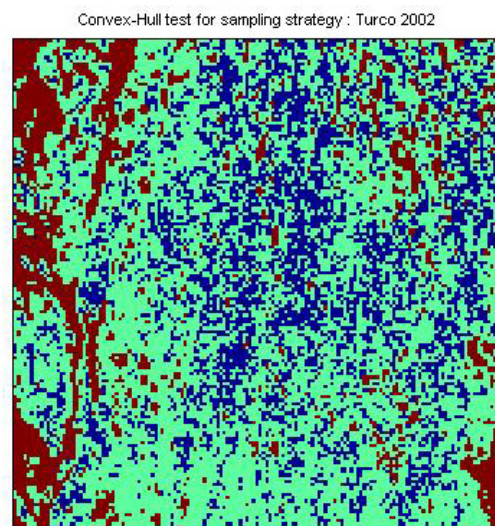

Figure 8. Evaluation of the sampling based on the convex hulls. The map is shown at the bottom: blue and light blue correspond to the pixels belonging to the 'strict' and 'large' convex hulls and red to the pixels for which the transfer function is extrapolating.

This map shows that the representativeness of the ESUs is quite good, even if pixels are outside the two convex-hulls. They mainly correspond to pixels where the NDVI values are the highest: grassland in the south-east, vegetation along the dry river and on the foothills in the west…

3. Determination of the transfer function for the 5 biophysical variables: LAItrue, LAI57eff, LAI57true, fCover, fAPAR

3.1. The transfer function considered

For each class determined in §2.3, the following transfer function was tested:

● REG: if the number of ESUs is sufficient, multiple robust regression between ESUs reflectance (or Simple Ratio) and the considered biophysical variable can be applied: we used the 'robustfit' function from the Matlab statistics toolbox. It uses an iteratively re-weighted least squares algorithm, with the weights at each iteration computed by applying the bisquare function to the residuals from the previous iteration. This algorithm provides lower weight to ESUs that do not fit well. The results are less sensitive to outliers in the data as compared with ordinary least squares regression. At the end of the processing, three errors are

computed: classical root mean square error (RMSE), weighted RMSE (using the weights attributed to each ESU) and cross-validation RMSE (leave-one-out method).

The regression is tested using either the reflectance or the logarithm of the reflectance for any band combination as well as the simple ratio or NDVI. As the method has poor extrapolation capacities, a flag image, based on the convex hulls is computing over reflectances.

3.2. Results

3.2.1. Choice of the method

For the 4 classes, a unique transfer function is computed. Figure 9 shows the results obtained for all the possible band combinations using either the reflectance (ρ) or the logarithm of the reflectance (log(ρ)): for LAItrue, LAI57eff, LAI57true, fCover and fAPAR, the results using the reflectance are selected since they provide the best results or compromises.

Depending on the biophysical variable, the choice of the method proves to be difficult because the results are very close. Note that the Red*NIR ('+' or RN) combination is added to all the band combinations (except for NDVI and SR). Please read the document: "A method to improve the relation between the biophysical variables" (http://www.avignon.inra.fr/valeri/table_methods/new_linear.pdf).
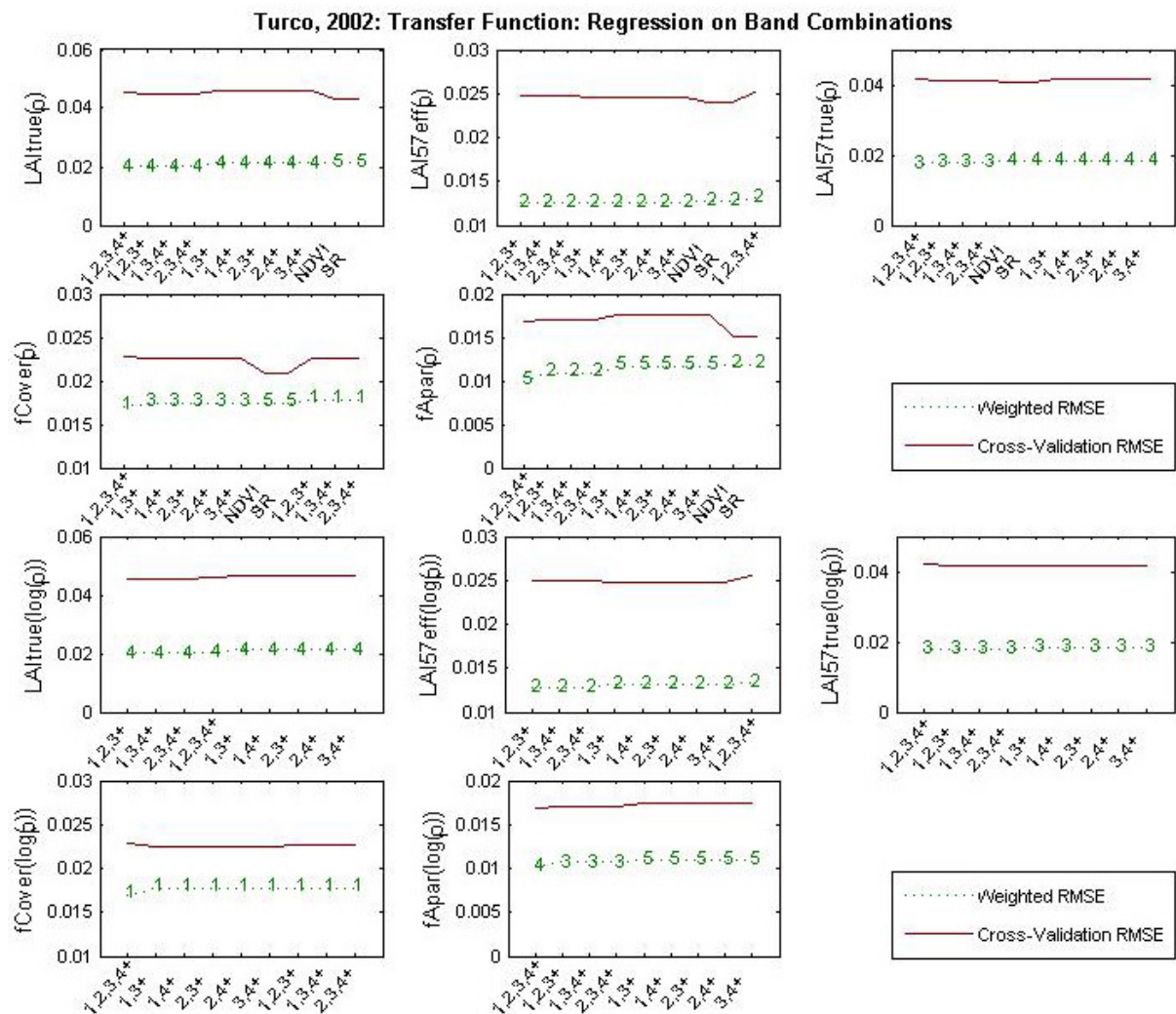

Figure 9. Transfer function: test of multiple regression applied on different band combinations. Band combinations are given in abscissa. The estimated biophysical variable is given in ordinate. Top graphs correspond to regression made on reflectance (ρ): the weighted root mean square error (RMSE) is presented in green along with the cross-validation RMSE in red. The numbers indicate the number of data used for the robust regression with a weight lower than 0.7 that could be considered as outliers. Bottom graphs correspond to regression made on the logarithm of the reflectance.

3.2.2. Choice of the band combination

The results obtained for all the possible band combinations using either the reflectance (ρ) or the logarithm of the reflectance ($\log(\rho)$) are generally very close or identical. The NDVI or the SR gives also similar results, but the number of weights lower than 0.7 is sometimes highest.

For the LAItrue, the XS2, XS3, XS4, RN (Figure 10 and Figure 11) combination on reflectance was selected: four weights are lower than 0.7 and the weighted RMSE value is the lowest. The following band combinations provide the same results: [XS1,XS2,XS3,RN], [XS1,XS3,XS4,RN].
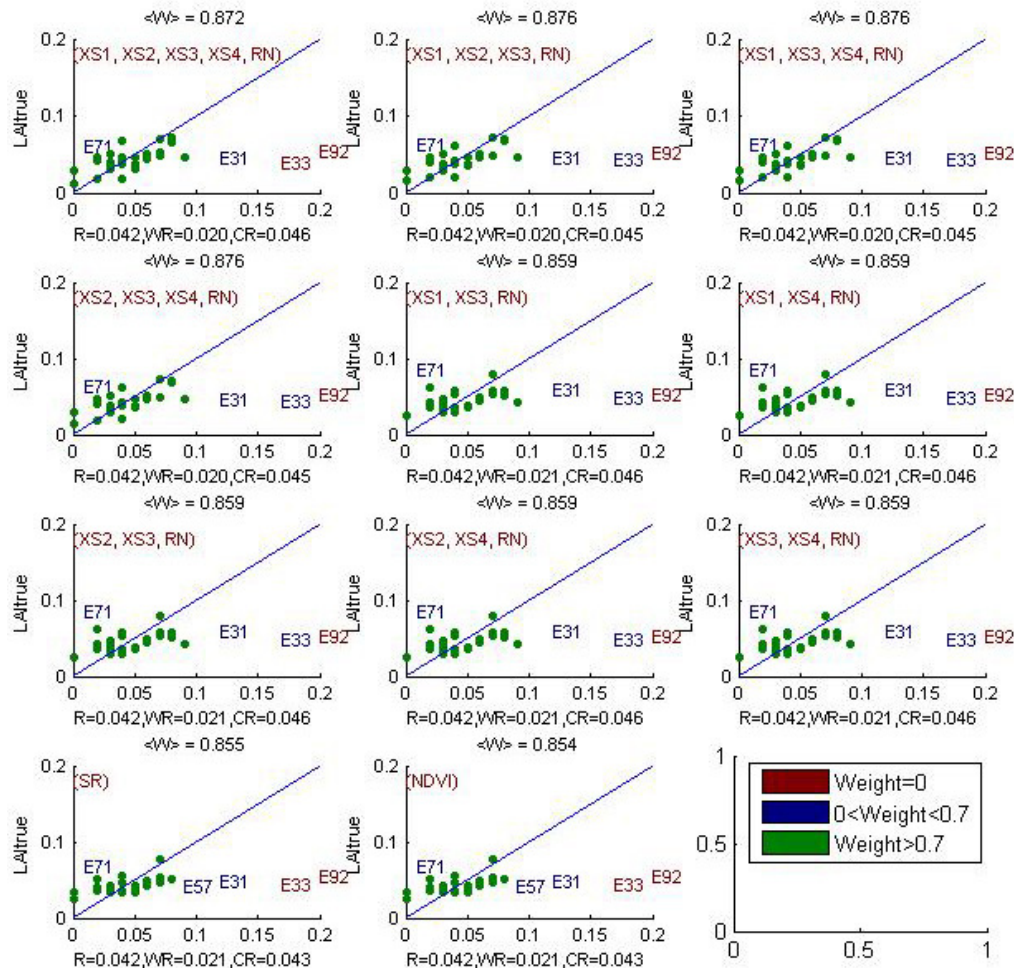

Figure 10. True Leaf Area Index: results for regression on reflectance using different band combinations. R is the root mean square error computed between LAItrue and estimated LAItrue. WR is the weighted root mean square error and CR is the cross validation root mean square error.
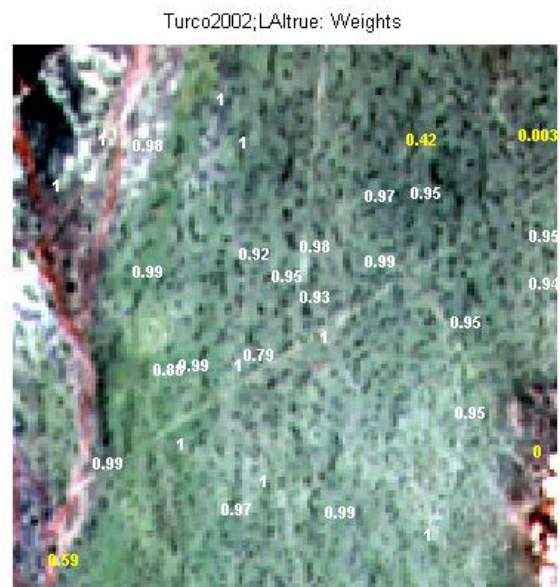
Figure 11. Weights associated to each ESU for the determination of LAItrue transfer function.

For the LAI57eff, the XS1, XS2, XS3, XS4, RN (Figure 12 and Figure 13) combination on reflectance was selected. Two weights are lower than 0.7. All the band combinations provide the same results, except NDVI and SR.
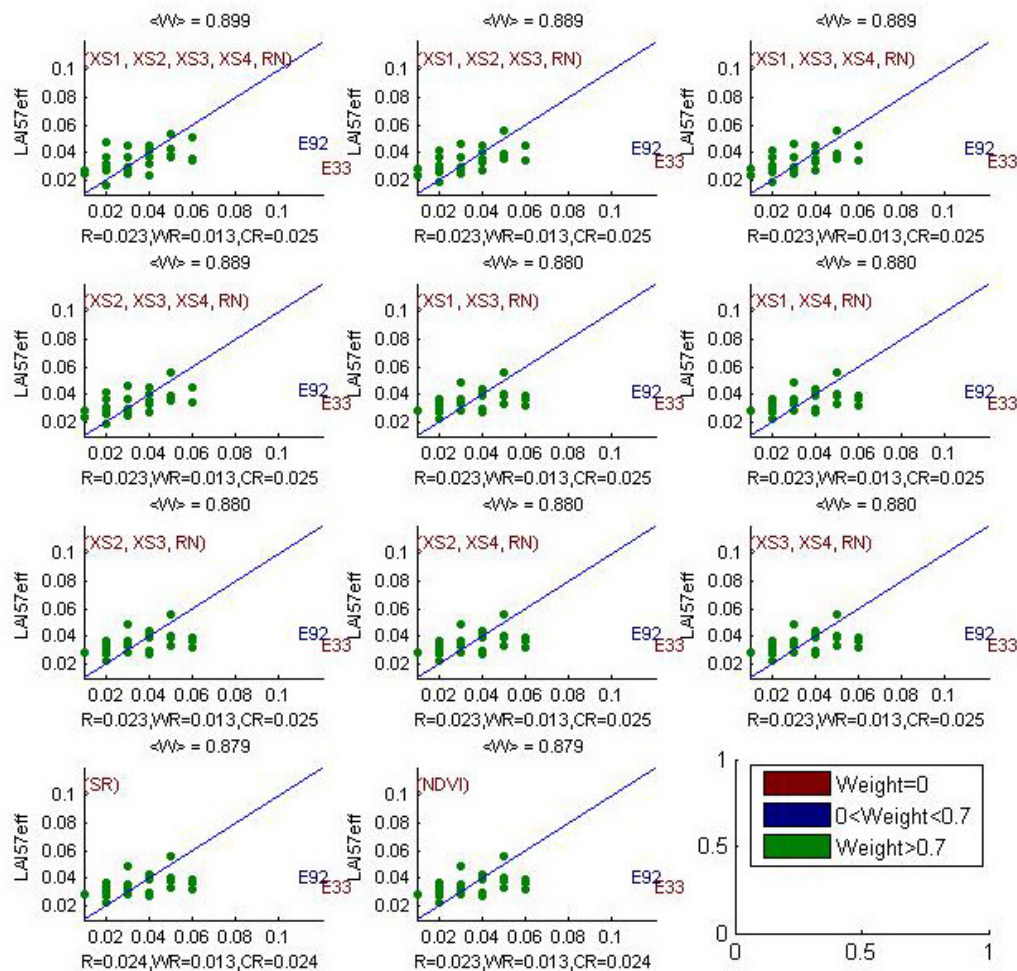
Figure 12. Effective LAI at 57.5°: results for regression on reflectance using different band combinations. R is the root mean square error computed between LAI57eff and estimated LAI57eff. WR is the weighted root mean square error and CR is the cross validation root mean square error.
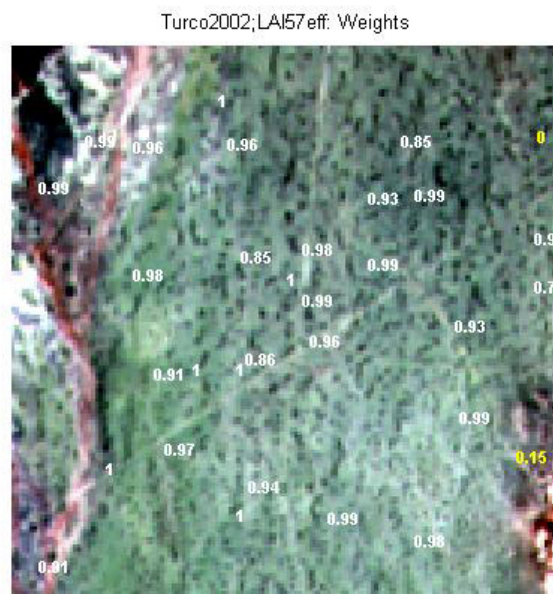

Figure 13. Weights associated to each ESU for the determination of LAI57eff transfer function.

For the LAI57true, the XS2, XS3, XS4, RN (Figure 14 and Figure 15) combination on reflectance was selected. Three weights are lower than 0.7 and the cross validation RMSE value is the lowest. All the band combinations provide the same RMSE and weighted RMSE.

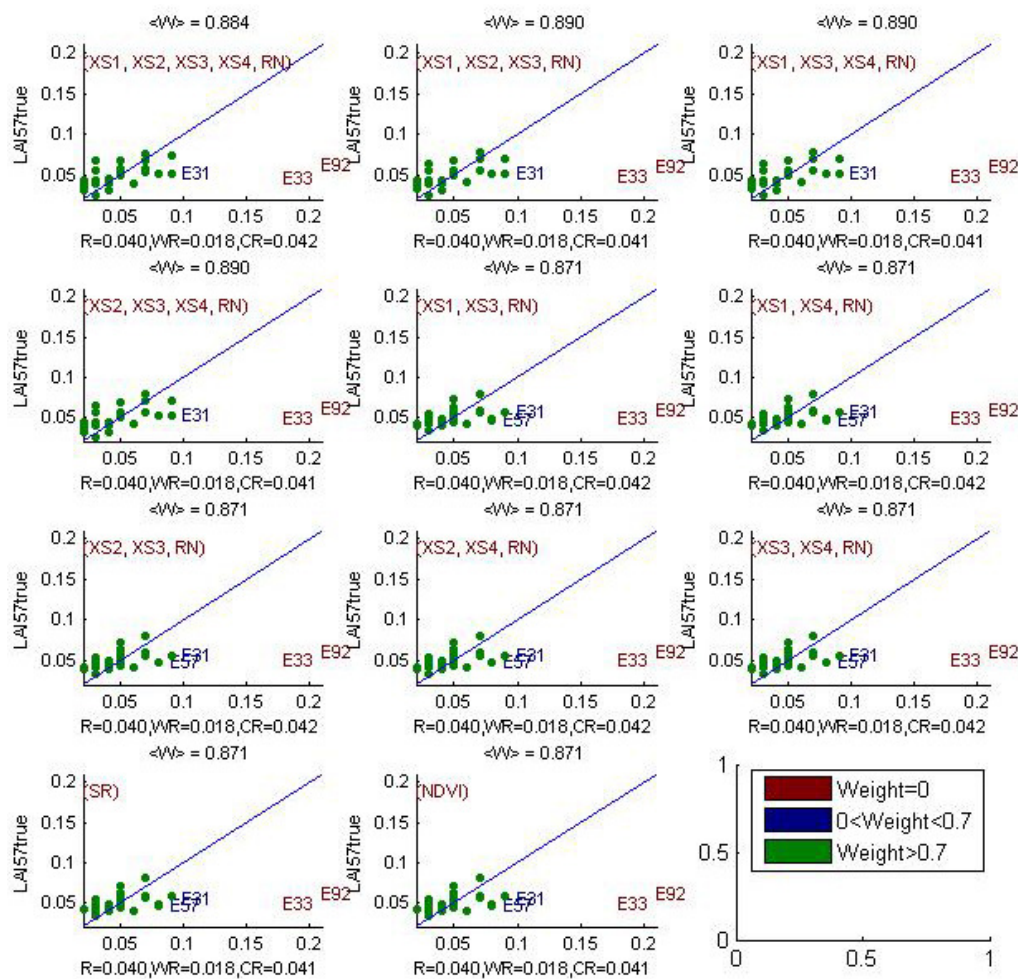**Figure 14. True Leaf Area Index at 57.5°: results for regression on reflectance using different band combinations. R is the root mean square error computed between LAI57true and estimated LAI57true. WR is the weighted root mean square error and CR is the cross validation root mean square error.**
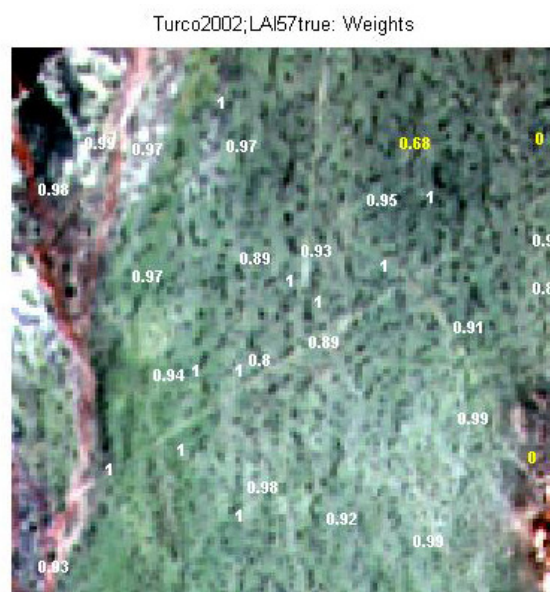

Figure 15. Weights associated to each ESU for the determination of LAI57true transfer function.

For the fCover, the XS1, XS2, XS3, XS4, RN (Figure 16 and Figure 17) combination on reflectance was selected since it provides a good compromise between the cross-validation RMSE, the number of weights lower than 0.7 and the weighted RMSE (the lowest value).
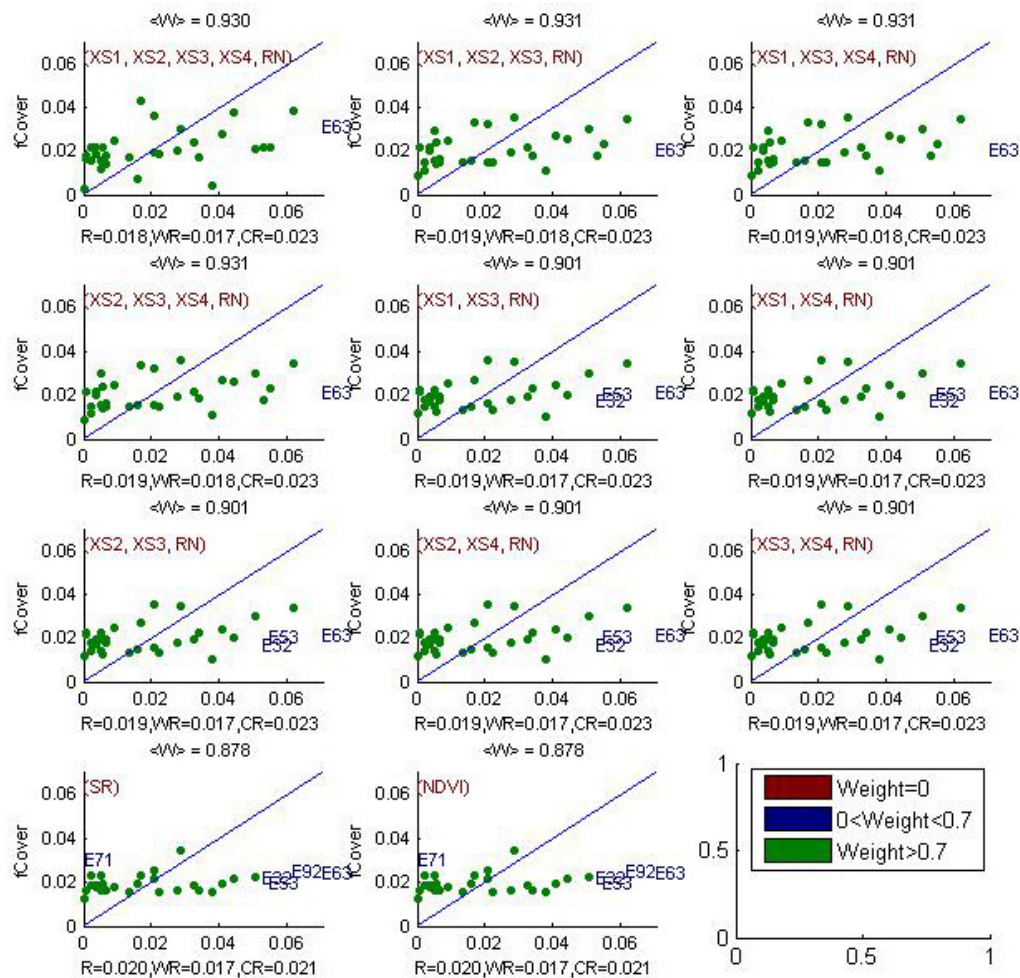

Figure 16. fCover: results for regression on reflectance using different band combinations. R is the root mean square error computed between fCover and estimated fCover. WR is the weighted root mean square error and CR is the cross validation root mean square error.

Figure 17. Weights associated to each ESU for the determination of fCover transfer function.

For the fAPAR, the XS2, XS3, XS4, RN (Figure 18 and Figure 19) combination on reflectance was selected since it provides a good compromise between the cross-validation RMSE, the number of weights lower than 0.7 (two) and the weighted RMSE. The following band combinations provide the same results: [XS1,XS2,XS3,RN]; [XS1,XS3,XS4,RN].

Figure 18. fAPAR: results for regression on reflectance using different band combinations. R is the root mean square error computed between fAPAR and estimated fAPAR. WR is the weighted root mean square error and CR is the cross validation root mean square error.
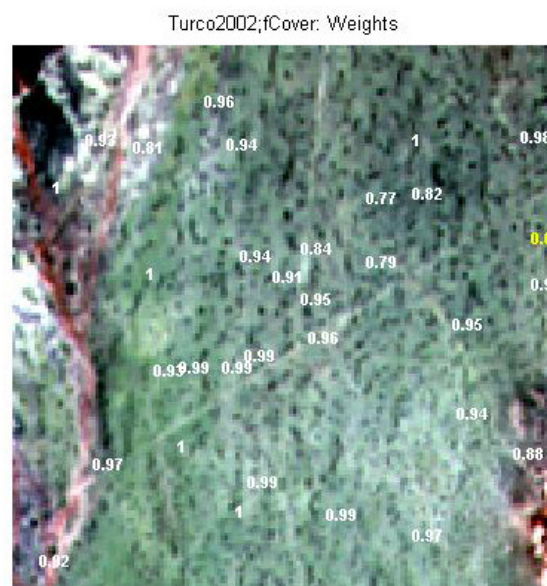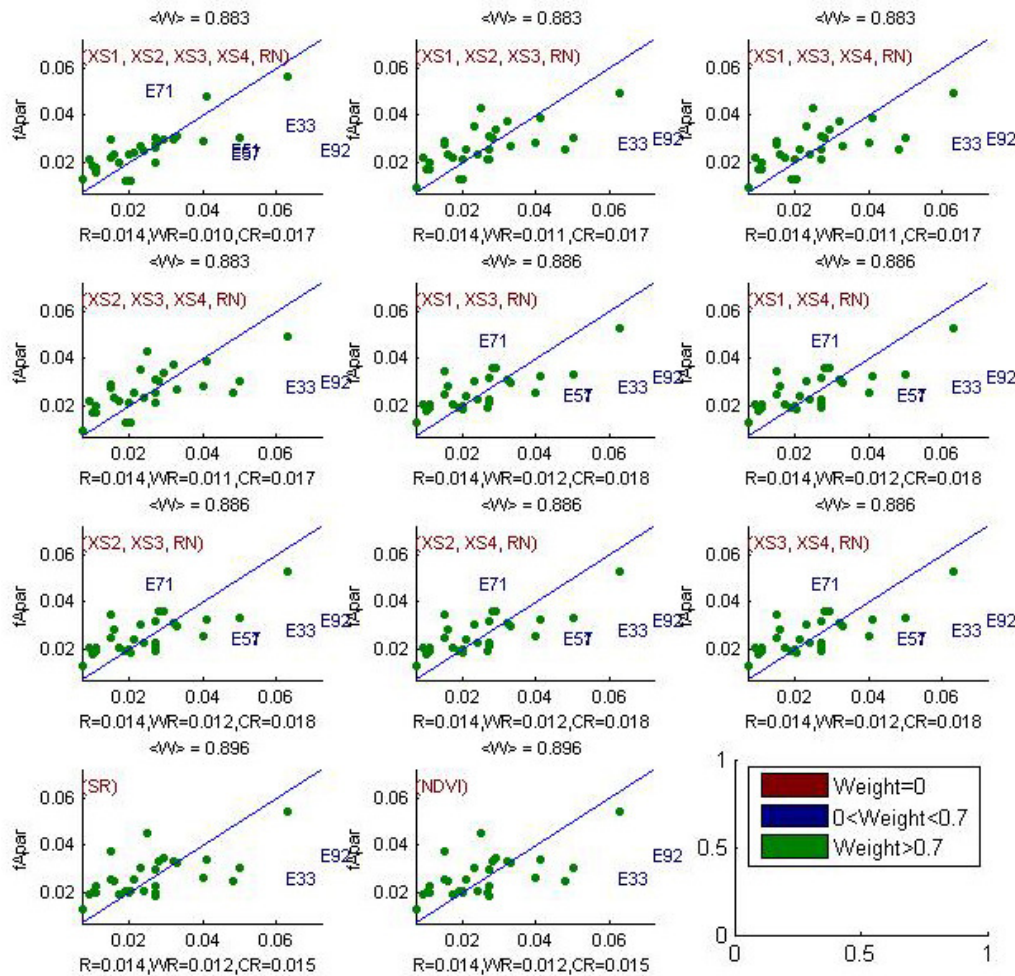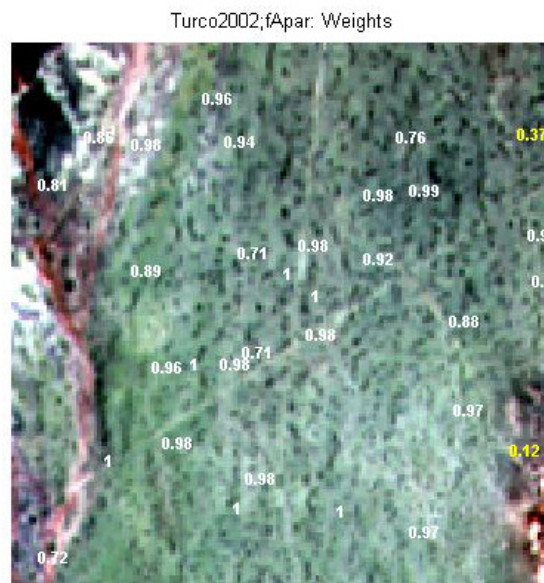

Figure 19. Weights associated to each ESU for the determination of fAPAR transfer function.

Following, the results of the transfer function (Table 2):

Variable	Band Combination	RMSE	Weighted RMSE	Cross-valid RMSE
LAItrue	- 8.1388 - 0.09933(XS2) + 36.963(XS3) + 36.786(XS4) - 167.52(RN)	0.042	0.020	0.045
LAI57eff	- 2.1948 + 0.31701(XS1) + 8.0741(XS2) + 11.983(XS3) - 0.36585(XS4) - 46.302(RN)	0.023	0.013	0.025
LAI57true	- 5.5219 + 0.045595(XS2) + 24.297(XS3) + 25.6(XS4) - 113.68(RN)	0.040	0.018	0.041
fCover	- 0.97169 + 0.080975(XS1) + 1.6042(XS2) + 8.2289(XS3) - 0.93947(XS4) - 22.145(RN)	0.018	0.017	0.023
fAPAR	- 2.9491 + 0.026382(XS2) + 12.816(XS3) + 14.029(XS4) - 61.866(RN)	0.014	0.011	0.017

RN = Red*NIR

Table 2. Transfer function applied to the whole site for the different biophysical variables, and corresponding errors

3.3. Applying the transfer function to the Turco SPOT image extraction

Figure 20 presents the biophysical variable maps obtained with the transfer function described in Table 2. The maps obtained for the five variables are consistent, showing similar patterns: low LAItrue values where low fCover or fAPAR are observed and conversely… The difference between effective LAI and true LAI is significant (see the average values in Figure 20). This was expected when looking the LAI57eff/LAI57true relationship, showing that for high LAI the difference between the two can be significant.

Figure 20. High resolution biophysical variable maps applied on the Turco site (top). Associated Flags are shown at the bottom: blue and light blue corresponds to the pixels belonging to the 'strict' and 'large' convex hulls and red to the pixels for which the transfer function is extrapolating.

The flag maps are comparable between LAItrue, LAI57true and fAPAR and between LAI57eff and fCover. This is due to the choice of the combinations[2]. Note that the pixels outside the strict convex hull correspond mainly to grassland in the south-east and vegetation along the dry river or on the foothills in the west.

---

[2] In theory, the more the number of bands increases, the larger the extrapolation is.

4. Conclusion

The transfer functions are obtained by using 32 ESUs. The representativeness of the land cover of the different ESUs is good. The results of the robust regression are also good and the maps obtained for the biophysical variables are consistent. The flag associated to each map show that the extrapolation of the transfer function is mainly bounded to grassland in the south-east and vegetation along the dry river or on the foothills in the west.

Note that the biophysical variable values are very low over the whole site. The LAIeff map is not available: the CAN-EYE software (V4.1) provides LAIeff values with a resolution of 0.1 while the resolution is equal to 0.01 for LAItrue, LAI57eff and LAI57true. For all the variables, the regression coefficients are computed by relating the variable itself to reflectance.

The biophysical variable maps are available in UTM, 19 South, projection coordinates (Datum: WGS-84) at 20 m resolution.

5. Acknowledgements

ANNEX

Ground measurements acquisition report for the VALERI site **Turco**

sampled from 25/08/2002 to 30/08/2002

Roland Bosseno
Organization: IRD/INRA-CSE, Avignon, France
email: rbosseno@avignon.inra.fr

Date of report 02/10/2002

People participating to the field experiment:

Firstname & Name	0rganization
Roland Bosseno	IRD/INRA CSE, Avignon, France
Sebastien Garrigues	INRA CSE, Avignon, France
Freddy Loza de la Cruz	ABTEMA, La Paz, Bolivia
Justina Mollo de Villca	Breeder, Turco, Bolivia
Rufián Villca Carex	Breeder, Turco, Bolivia

Site coordinates

	Lat-Long PSAM56 (Deg min.00)		UTM / WGS84 UTM		Other projection*	
	Lat.	Long.	Easting	Northing	Easting	Northing
Upper left corner	18°13.3370 S	68°12.9877 W			584000	7985000
Lower right corner	18°14.9674 S	68°10.6250 W			587000	7982000

*The other projection user is UTM19S-PSAM56. All the characteristics are provided in the following table (see http://www.avignon.inra.fr/valeri/, methodology page, GPS document for more information):

Geodesic Map Datum	
Associated Ellipsoïd	international 1924
Semi-major axe	6378388
Semi-minor axe	6356911.9
1/flattening	297
Eccentricity	0.081991978

Ground control points

	Easting	Northing	Comments
wp1	584055	7982403	artificial circular hole
wp2	584503	7984521	artificial circular hole
wp3	584459	7984444	deep old road
wp4	585723	7986842	new road intersection
wp5	585447	7986035	artificial circular hole
wp6	585728	7985608	new road intersection
wp7	584316	7985101	old road
wp8	584459	7984444	old road

GPS system used: Garmin etrex.
Typical uncertainty of GPS position: 8 m.

Description of the site and land cover

Category according to IGBP classification
Barren and sparsely vegetated.

Comments on the land cover
The land cover is composed only of:
Tholar which are a homogeneous population of shrub (festuca ortophylla). The plant has 1 meter height maximum. The fraction of plant cover is runing between 5 and 20 %. Soil surface has a sandy texture and pale brown color 10YR6/3 (Munsell Soil Color Charts), it is covered by a discontinue moquet of short grass, dry during this season, and by some brown gravel (10YR5/3).
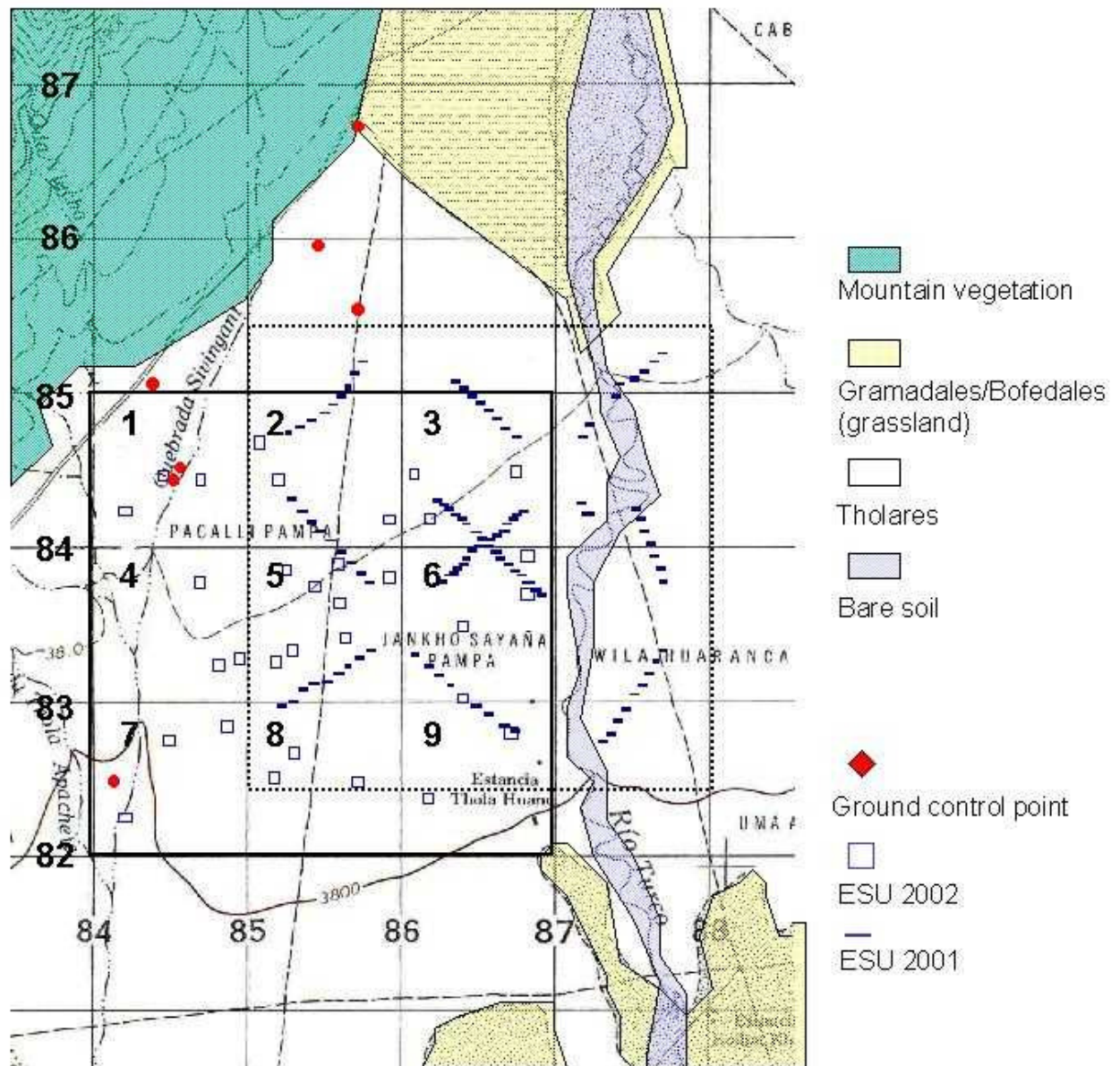The SPOT image was acquired the 29/08/2002 during the ground measurements.

Topography
The site is at about 3800 m altitude. It is absolutely flat, with a very small slope of 0.5 % in the South East direction.

Land cover map
The land cover map included here is approximative and should be refined according to the SPOT image.
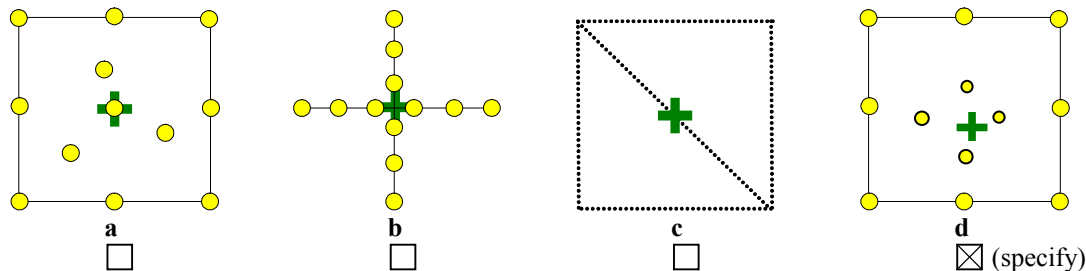
Spatial Sampling scheme

Sensors used for sampling the ESUs

	Method	Comments
☒	Hemispherical photographs	NIKON Coolpix9000 instruments
☐	LAI2000	
☐	TRAC	
☐	Ceptometer	
☐	Direct measurements	
☒	Other	fCOVER, Green biomass and LAI also was estimated by direct and destructive measurements.

Sampling strategy for the ESU

a	b	c	d
☐	☐	☐	☒ (specify)

Distribution of the Elementary sampling units

The distribution of the ESUs was obtained by a random algoritme, because all part of site has a easy accessibiity and show only one kind of land cover .

Each ESUs was not too close to the borders of the one km pixel (at least 40 to 50m).

32 ESUs were sampled, 8 in the central pixel and 3 in each periferical pixels.

The high spatial resolution image

Satellite

Satellite used   SPOT4 HRVIR1
Level of processing   SpotView Basic
Projection type   UTM19S
Datum: PSAM56
Georeferencing accuracy: 1 to 2 pixels (95 % of confidence).

List of the ESUs

ESU	Month	Day	Hour	Minute	UTM-E	UTM-N	Team	Comments
11	08	28	15	47	584126	7984225	A	Tholar
12	08	28	15	23	584400	7984477	"	"
13	08	28	14	54	584653	7984442	"	"
21	08	28	13	00	585050	7984704	"	"
22	08	28	13	30	585175	7984449	"	"
23	08	27	15	11	585942	7984161	"	"
31	08	27	15	45	586124	7984485	"	"
32	08	27	14	43	586218	7984173	"	"
33	08	27	14	18	586802	7984505	"	"
41	08	29	11	15	584641	7983739	"	"
42	08	26	14	15	584766	7983188	"	"
43	08	26	11	00	584908	7983224	"	"
51	08	29	12	30	585251	7983828	"	"
52	08	25	14	00	585589	7983869	"	"
53	08	28	09	38	585941	7983790	"	"
54	08	28	10	00	585596	7983603	"	"
55	08	28	10	20	585426	7983717	"	"
56	08	26	09	35	585637	7983372	"	"
57	08	26	10	15	585271	7983281	"	"
58	08	26	10	40	585160	7983216	"	"
61	08	27	16	39	586436	7983456	"	"
62	08	27	13	45	586875	7983680	"	"
63	08	27	13	00	586872	7983928	"	"
71	08	26	15	35	584131	7982133	"	"
72	08	26	14	45	584432	7982677	"	"
73	08	26	13	50	584823	7982773	"	"
81	08	26	16	30	585148	7982417	"	"
82	08	27	08	38	585296	7982584	"	"
83	08	27	09	20	585723	7982391	"	"
91	08	27	11	00	586447	7982949	"	"
92	08	27	10	28	586764	7982728	"	"
93	08	27	11	34	586201	7982285	"	"

This is extracted from the Excel file turco2002gps.xls.

Acknowledgements